

# 1 **A global analysis of reconstructed land climate changes during Dansgaard-** 2 **Oeschger events**

3 Mengmeng Liu<sup>1,2,\*</sup>, Iain Colin Prentice<sup>1</sup>, Sandy P. Harrison<sup>2</sup>

4 1: Georgina Mace Centre for the Living Planet, Department of Life Sciences, Imperial College  
5 London, Silwood Park Campus, Buckhurst Road, Ascot SL5 7PY, UK

6 2: Department of Geography and Environmental Science, University of Reading, Reading,  
7 RG6 6AB, UK

8 **\* Corresponding author: [m.liu18@imperial.ac.uk](mailto:m.liu18@imperial.ac.uk)**

9 Ms for: *Climate of the Past*

## 10 **Abstract**

11 Dansgaard–Oeschger (D–O) warming events are comparable in magnitude and rate to the  
12 anticipated 21st century warming. As such, they provide a good target for evaluation of the  
13 ability of state-of-the-art climate models to simulate rapid climate changes. Despite the wealth  
14 of qualitative information about climate changes during the D–O events, there has been no  
15 attempt to date to make quantitative reconstructions globally. Here we provide reconstructions  
16 of seasonal temperature changes and changes in plant-available moisture across multiple D–O  
17 events during Marine Isotope Stage 3 based on available pollen records across the globe. These  
18 reconstructions show that the largest warming occurred in northern extratropics, especially  
19 Eurasia, while western North America and the southern extratropics were characterised by  
20 cooling. The change in winter temperature was significantly larger than the change in summer  
21 temperature in the northern extratropics, indicating that the D–O warming events were  
22 characterised by reduced seasonality, but there is no significant difference between the summer  
23 and winter temperature changes in the southern extratropics and the tropics. The antiphasing  
24 between northern and southern extratropical changes, and the west-east pattern of cooling and  
25 warming in North America are consistent across the eight D–O events examined, although the  
26 signal at individual sites may vary between events. Globally, changes in moisture were  
27 positively correlated with changes in temperature, but the strength and the sign of this  
28 relationship vary regionally. These reconstructions can be used to evaluate the spatial patterns

29 of changes in temperature and moisture in the transient simulations of the D-O events planned  
30 as part of the Palaeoclimate Modelling Intercomparison Project.

## 31 1. Introduction

32 Dansgaard–Oeschger (D–O) events are characterised in Greenland by a transition from cold  
33 Greenland Stadial (GS) to warmer Greenland Interstadial (GI) conditions (Dansgaard et al.,  
34 1993). The surface air temperature in Greenland increased by 10–15° C during the warming  
35 phases; these warming events occur over an interval of between 50 and 200 years (Huber et  
36 al., 2006; Kindler et al., 2014). Thus, the D-O events offer a parallel in terms of speed to  
37 projected future warming, although both the baseline state and the mechanism inducing this  
38 warming differ from anticipated 21st century climate changes. D-O events could therefore  
39 provide an opportunity to determine how well climate models that are used for future  
40 projections can simulate rapid climate changes (Malmierca-Vallet et al., 2023), particularly  
41 regional patterns of warming (and cooling) that are regarded as a challenge for modelling  
42 (Doblas-Reyes et al., 2021; Lee et al., 2021) and are highly important in assessing the  
43 vulnerability of human societies to future climate changes (IPCC 2022).

44 D-O events are registered globally (Voelker, 2002; Sánchez Goñi and Harrison, 2010; Harrison  
45 and Sánchez Goñi, 2010; Sánchez Goñi et al., 2017; Adolphi et al., 2019; Corrick et al., 2020).  
46 Shifts in vegetation types between GI and GS states have been interpreted as primarily a  
47 temperature signal in the extratropics and a moisture signal in the tropics (Harrison and  
48 Sánchez Goñi, 2010). Speleothem records provide a good time-control on the synchronicity of  
49 climate changes globally with the D-O events registered in Greenland (Adolphi et al., 2019;  
50 Corrick et al., 2020), but the driver of this signal can either be temperature or precipitation  
51 depending on the region. There are quantitative climate reconstructions based on terrestrial  
52 pollen records from La Grande Pile (Guiot et al., 1993), Lago Grande di Monticchio (Huntley  
53 et al., 1999), Padul (Camuera et al., 2022), El Cañizar de Villarquemado (Wei et al., 2021;  
54 Camuera et al., 2022) and Lake Ohrid (Sinopoli et al., 2019), marine cores in the western  
55 Mediterranean and offshore from Portugal (Sánchez-Goñi et al., 2002), diatom assemblages at  
56 Les Echets, France (Ampel et al., 2010), bacterial membrane lipid records from the Eifel region  
57 (Zander et al., 2023), isotopic measurements of earthworm calcite from the Rhine Valley  
58 (Prud'homme et al., 2022) and clumped isotope measurements on snails in Hungary (Újvári et  
59 al., 2021). Aside from the lack of comparable quantitative estimates from outside Europe,  
60 differences in the methodology employed and in the specific climate variables reconstructed in  
61 each of these studies limits their usefulness for model evaluation. In particular, given that there  
62 is still uncertainty as to whether the D-O cycles are characterised by changes in seasonality

63 such that warming events are primarily driven by changes in winter (Flückiger et al., 2008;  
64 Zander et al., 2024), in the regional strength of the warming (Harrison and Sánchez Goñi, 2010)  
65 and how warming relates to changes in moisture (Wei et al., 2021), there is a need for more  
66 systematic reconstruction of seasonal climate changes.

67 In the paper, we provide reconstructions of seasonal temperature changes and changes in plant-  
68 available moisture during the intervals corresponding to D-O warming events in Greenland  
69 during Marine Isotope Stage 3 based on available pollen records globally. We employ a  
70 standard methodology to construct age models for these records, as well as a standard  
71 regression-based approach to make the reconstructions. We analyse the regional patterns to  
72 identify key targets for model evaluation.

## 73 **2. Methods**

### 74 **2.1. Data sources**

75 Modern pollen data were obtained from version 2 of the SPECIAL Modern Pollen Data Set  
76 (SMPDSv2: Villegas-Diaz and Harrison, 2022). This global data set contains 24649 modern  
77 pollen records from 17827 sites. The dataset contains relative abundance records for 4816  
78 pollen taxa, created after removing taxa that are not climatically diagnostic (e.g. obligate  
79 aquatics, carnivorous species, cultivated plants). The data set provides several levels of  
80 taxonomic aggregation; here we use the most aggregated level, where woody species were  
81 generally combined at genus level and herbaceous species at sub-family or family level unless  
82 they were palynologically distinctive, occupied distinctive ecological niches and were  
83 sufficiently geographically widespread. This "amalgamated" data set contains relative  
84 abundance information for 1338 taxa. These samples were aggregated by longitude, latitude  
85 and elevation in order to remove duplicates. Counts for *Quercus*, *Quercus* (deciduous) and  
86 *Quercus* (evergreen) were combined because of inconsistent differentiation of *Quercus* pollen  
87 in different regional records. Deciduous and evergreen oaks occupy different areas of climate  
88 space, particularly in terms of seasonal moisture; specifically, evergreen oaks are typically  
89 found in areas characterised by winter rainfall such as the Mediterranean. Nevertheless, since  
90 there are other plant taxa that are similarly diagnostic of such regimes, the amalgamation of  
91 *Quercus* (deciduous) and *Quercus* (evergreen) should not have a major effect on the robustness  
92 of our climate reconstructions. Taxa that occurred in less than 10 samples in the training data  
93 set were not used to make reconstructions because it is unlikely that the available samples

94 provided a reasonable estimate of the climate space occupied by these rare taxa (Liu et al.,  
95 2020). After filtering, the data set contains information on 591 individual pollen taxa from  
96 17547 sites (Figure 1).

97 The SMPDSv2 also provides climatic information at each pollen site, specifically the mean  
98 temperature of the coldest month (MTCO), mean temperature of the warmest month (MTWA),  
99 and a plant-available moisture ~~moisture index~~ ( $\alpha$ ) calculated as the ratio of actual  
100 evapotranspiration to equilibrium evapotranspiration.  $\alpha$  is a transformation of the commonly  
101 used moisture index MI, to emphasize the differences at the dry end of the climate range, which  
102 have a more pronounced effect on vegetation distribution than differences at the wet end  
103 (Prentice et al., 2017). Detailed relationships are in Supplementary Materials. These bioclimate  
104 variables reflect mechanistically distinct controls on plant growth.

105 The fossil pollen data were obtained from the Abrupt Climate Changes and Environmental  
106 Responses (ACER) database (Sánchez Goñi et al., 2017), which includes 93 records from the  
107 last glacial period (73-15 ka) with sufficient resolution and dating control to detect sub-  
108 millennial scale variability. Here we focus on the 73 records covering most of Marine Isotope  
109 Stage 3 (50-30 ka); 54 of these records are from terrestrial sites and 19 from marine sites  
110 (Figure 1; Table 1). The fossil data were taxonomically harmonised to be consistent with the  
111 SMPDSv2.

112 We have used a global pollen data set for calibration of the pollen-climate relationships,  
113 SMPDSv2 (Villegas-Diaz and Harrison, 2022). The use of a global data set, rather than region-  
114 specific training data, relies on the principle of phylogenetic niche conservatism (Harvey and  
115 Pagel, 1991), which states that traits tend to remain constant over time. This also applies to the  
116 climate niche (Wiens and Graham, 2005; Wiens et al., 2010; Peterson, 2011; Crisp and Cook,  
117 2012; Jiang et al., 2023) as evidenced by disjunct distributions of taxa across different  
118 continents (Yin et al., 2021). Niche conservatism underpins the fact that the modern  
119 distribution of specific genera can be predicted using climate-pollen relationships developed  
120 from other regions (e.g. Huntley et al., 1989). The use of a global data set for calibration makes  
121 it possible to sample a large range of climates, and thus makes it more likely that the  
122 reconstructions of glacial climates are realistic and not confined to the limited climate range  
123 sampled in any one region (Turner et al., 2020). Indeed, Turner et al. (2020) have shown that  
124 increasing the size of the calibration data set tends to lead to smaller reconstruction errors and

125 more accurate estimates of taxon coefficients. Pragmatically, the use of a global data set also  
126 facilitates making reconstructions for sites from regions where there is limited modern pollen  
127 data.

## 128 **2.2. Climate reconstruction method**

129 We used tolerance-weighted Weighted Averaging Partial Least Squares (*fxTWA-PLS*: Liu et  
130 al., 2020; Liu et al., 2023) regression to model the relationships between taxon abundances and  
131 individual climate variables in the SMPDSv2 modern training dataset and then applied these  
132 relationships to reconstruct past climate using the fossil assemblages from the ACER database  
133 (Figure 2). *fxTWA-PLS* reduces the tendency of regression methods to compress  
134 reconstructions towards the centre of the sampled climate range by applying a sampling  
135 frequency correction to reduce the influence of uneven sampling of climate space and  
136 weighting the contribution of individual taxa according to their climate tolerances (Liu et al.,  
137 2020). Version 2 of *fxTWA-PLS* (*fxTWA-PLS2*, Liu et al., 2023) uses P-splines smoothing to  
138 derive the frequency correction and applies this correction both in estimating the climate  
139 optima and tolerances, and in the regression itself, producing a further improvement in model  
140 performance compared to version 1 (Liu et al., 2020).

141 We evaluated the *fxTWA-PLS* models by comparing the reconstructions with observations  
142 using leave-out cross-validation, where one site at a time was randomly selected as a test site  
143 and sites that are both geographically close (within 50 km horizontal distance from the site)  
144 and climatically close (within 2% of the full range of each climate variable in the dataset) were  
145 removed from the training set along with this test site, to prevent redundancy in the climate  
146 information from inflating the cross-validation goodness of fit, following Liu et al. (2020). We  
147 selected the last significant number of components ( $p$ -value  $\leq 0.01$ ) and assessed model  
148 performance using the root mean square error of prediction (RMSEP). Compression was  
149 assessed using linear regression of the leave-out cross-validated reconstructions on to the  
150 climate variable. Reconstructions of MTCO, MTWA and  $\alpha$  were made for every sample in  
151 each fossil record. Sample specific errors were estimated via bootstrapping, as described in Liu  
152 et al. (2020). We corrected for the effect of changes in atmospheric CO<sub>2</sub> on plant water-use  
153 efficiency, and hence the reconstructions of  $\alpha$  (Figure S1), following Prentice et al. (2022).  
154 Appropriate values of CO<sub>2</sub> were taken from the WAIS Divide ice core record (Bauska et al.,  
155 2021).

### 156 2.3. Age modelling

157 Although the ACER database provides age models for each pollen record, the resolution of the  
 158 individual records is variable (mean resolution 474 years) and these models are often  
 159 imperfectly aligned with the dating of D-O events as recorded in the Greenland ice core, and  
 160 which have been shown to have a globally synchronous imprint through analysis of speleothem  
 161 records (Adolphi et al., 2019; Corrick et al., 2020). To create a better alignment, we used  
 162 dynamic time warping (DTW: Belman and Kalaba, 1959; Burstyn et al., 2021) to adjust the  
 163 age scale for each individual record (Figure 2). Dynamic time warping optimises the similarity  
 164 between two sequences by stretching or compressing one sequence in the time dimension to  
 165 match the other. Here, we use simulated mean annual temperature (MAT) from a transient  
 166 simulation of the interval 50-30 ka made with the LOVECLIM model (Menviel et al., 2014)  
 167 as the reference sequence compared to MAT calculated as the average of MTCO and MTWA  
 168 from the individual pollen records. We used the mid-point between the start dates of each D-O  
 169 event (Wolff et al., 2010; converted into AICC2012 timescale) to sub-divide each ACER  
 170 record into discrete intervals and modified the time scale of the reconstructed mean annual  
 171 temperature series in each interval to match the reference sequence, having normalised both  
 172 sequences to remove the influence of differences in absolute values and the amplitude of  
 173 changes. The adjusted age model for each ACER record was then applied to the reconstructions  
 174 of MTCO, MTWA, and  $\alpha$  from that record for subsequent analyses.

### 175 2.4. Assessment of regional climate changes during Greenland D-O warming events

176 The magnitude of climate change during the interval corresponding to each D-O warming event  
 177 as registered in Greenland is calculated individually for each climate variable at each site. To  
 178 avoid making an assumption about the sign of the climate change at a site, we used a third-  
 179 order polynomial to fit the reconstructions during the interval from 300 years before to 600  
 180 years after the official start date corresponding to Greenland D-O warming for each event  
 181 (Wolff et al., 2010; converted into AICC2012 timescale) to determine whether the change was  
 182 positive or negative. We used the ages corresponding to the minimum and maximum in the  
 183 fitted polynomial ( $t_{\min \text{ polynomial}}$ ,  $t_{\max \text{ polynomial}}$ ) but restrict  $t_{\min \text{ polynomial}}$  and  $t_{\max \text{ polynomial}}$  to be found  
 184 at where there are reconstructions. ~~S~~However, since the smoothed polynomial may  
 185 underestimate or overestimate the amplitude of change, we used the reconstructed minimum

186 or maximum value within the period  $t_{\min \text{ polynomial}} \pm 100$  years or  $t_{\max \text{ polynomial}} \pm 100$  years  
 187 respectively (see Figure S2 [for illustration](#)).

188 In cases where no change was registered for all of the three climate variables, we assume that  
 189 the event was not registered at the site. As a measure of the accuracy of the DTW method to  
 190 identify D-O events, we compared the number of identified events with the number of D-O  
 191 events that [should](#) ~~occurred~~ during the time covered by each record (Table 1). To assess  
 192 whether events were missed in a particular record due to low sampling resolution, we examined  
 193 the number of samples present in the 900-year interval covering the sampled D-O (i.e. 300  
 194 years before to 600 years after the official start date of each event), where low resolution was  
 195 defined as  $\leq 3$  samples in this 900-year interval. Reconstructions covering intervals where a  
 196 signal was not identified were not used in subsequent analyses.

197 We calculated sample-specific errors for the minimum and maximum reconstructed values.  
 198 Assuming that the minimum and maximum values are independent, we used error propagation  
 199 to obtain the error of the change:

$$200 \quad \sigma_{\text{change}} = \sqrt{\sigma_{\min}^2 + \sigma_{\max}^2}$$

201 Following Liu et al. (2022), we used a maximum likelihood method to estimate the ratio of  
 202  $\Delta\text{MTCO}$  to  $\Delta\text{MTWA}$  (and ratio of  $\Delta\alpha$  to  $\Delta\text{MTWA}$ ) to take account of the errors on both  
 203 variables.

### 204 3. Results

205  $fx\text{TWA-PLS}$  reproduces the modern climate reasonably well (Table 2; [Figure S3](#)). The  
 206 performance is best for MTCO ( $R^2 \equiv 0.75$ ,  $\text{RMSEP} \equiv 6.51$ ,  $\text{slope} \equiv 0.85$ ) but is also good for  
 207 MTWA ( $R^2 \equiv 0.59$ ,  $\text{RMSEP} \equiv 3.68$ ,  $\text{slope} \equiv 0.71$ ) and  $\alpha$  ( $R^2 \equiv 0.65$ ,  $\text{RMSEP} \equiv 0.18$ ,  $\text{slope} \equiv$   
 208  $0.71$ ). Assessment of the variance inflation factor scores shows that there is no problem of  
 209 multicollinearity so that it is possible to reconstruct all three climate variables independently  
 210 (Liu et al., 2023).

211 The use of dynamic time -warping made it possible to identify D-O events robustly ([Figure](#)  
 212 [S4.1 ~ S4.8](#); Table 1; Supplementary Table 1). Thirteen of the 73 sites cover some part of the  
 213 50-30 ka periods but do not include D-O events. Across the remaining 60 sites, we identified

214 2978 out of the 348 individual D-O events (86.0%) that ~~occurred~~ should occur during the  
 215 intervals covered by the records. In the majority of cases where a D-O event should have been  
 216 registered but could not be identified in an individual record (4460 out of 5070 cases), the  
 217 resolution of that part of the record was extremely poor ( $\leq 3$  samples in the 900-year interval  
 218 starting 300 years before to 600 years after the official start date of the event).

219 Changes in both MTCO and MTWA were generally largest in the extratropics and were more  
 220 muted in the tropics (Figure 3). The change in MTCO was significantly larger in the northern  
 221 extratropics when considered across all D-O events and sites; the change in MTCO was larger,  
 222 but not significantly larger, in the southern extratropics and ; the changes in MTCO are not  
 223 correlated with the changes in MTWA in the tropics (Table 3). There is a significant positive  
 224 relationship between the change in  $\alpha$  and the change in MTWA in all regions (Figure 4; Table  
 225 4).

226 The spatial patterns of changes in MTCO and MTWA show consistent features across multiple  
 227 D-O events (Figure 5), most noticeably that the largest warming occurs in the extratropics of  
 228 Eurasia, while western North America and the southern extratropics are characterised by  
 229 cooling. The anti-phasing between the northern and southern extratropics is consistent across  
 230 D-O events. Nevertheless, both the magnitude of the changes and the spatial patterns vary  
 231 between the D-O events (Figure S5.13; Figure S4S5.2). Changes in  $\alpha$  broadly follow the  
 232 changes in temperature, with increased  $\alpha$  in regions characterised by warming (Figure 5) but  
 233 show more variability both spatially and between D-O events (Figure S5.35). This is  
 234 particularly true for Europe, which is characterised by a mixed signal of drying and wetting  
 235 (Figure S5.3).-

#### 236 4. Discussion and Conclusions

237 We have presented a first attempt to map the spatial patterns of quantitative changes in seasonal  
 238 temperature and plant-available moisture during D-O events globally, using a consistent  
 239 methodology and a single data source. These analyses show that there is an anti-phasing  
 240 between changes in the northern extratropics and the southern extratropics, with warming in  
 241 the north and cooling in the south. The largest and most consistent warming during D-O events  
 242 occurs in Eurasia. There is a significant difference in the warming during winter and summer  
 243 in the northern extratropics, resulting in an overall reduction in seasonality, but no significant  
 244 difference in the tropics and southern extratropics. Site-based reconstructions (e.g. Denton et

245 al., 2022; Zander et al., 2024) suggest much larger cooling in winter than summer during cold  
246 phases of the last glacial, implying enhanced seasonality compared to warm intervals, which  
247 would be consistent with our reconstructions of a reduction in seasonality during warming  
248 events in the northern extratropics. Globally, there is a positive relationship between the change  
249 in temperature and plant available moisture, as indicated by  $\alpha$ . This is consistent with more  
250 qualitative interpretation of palaeo-records from specific regions, where many regions are  
251 characterised by both warming and wetting (e.g. western Europe: Sánchez Goñi et al., 2008;  
252 Fletcher et al., 2010; eastern Europe: Fleitmann et al., 2009; Stockehecke et al., 2016; central  
253 Siberia: Grygar et al., 2006; the Great Basin USA: Denniston et al., 2007; Jiménez-Moreno et  
254 al., 2010). However, according to our reconstructions, the nature of this relationship varies  
255 between regions: there are some regions that are characterised by warming and wetting, others  
256 are characterised by warming and drying (Figure 4, Figure 5). Previous studies have also  
257 indicated drier conditions during D-O events, particularly in parts of the USA such as the  
258 Pacific Northwest (Grigg and Whitlock, 2002) and Florida (Grimm et al., 2006; Jiménez-  
259 Moreno et al., 2010). Although there is some consistency in the broadscale patterns of changes  
260 across D-O events, the magnitude of the changes as well as the spatial patterning varies  
261 between events (Figure S5.1~ 5.3).

~~262 We have used a global pollen data set for calibration of the pollen-climate relationships,  
263 SMPDsv2 (Villegas-Diaz and Harrison, 2022). The use of a global data set, rather than region-  
264 specific training data, relies on the principle of phylogenetic niche conservatism (Harvey and  
265 Pagel, 1991), which states that traits tend to remain constant over time. This also applies to the  
266 climate niche (Wiens and Graham, 2005; Wiens et al., 2010; Peterson, 2011; Crisp and Cook,  
267 2012; Jiang et al., 2023) as evidenced by disjunct distributions of taxa across different  
268 continents (Yin et al., 2021). Niche conservatism underpins the fact that the modern  
269 distribution of specific genera can be predicted using climate-pollen relationships developed  
270 from other regions (e.g. Huntley et al., 1989). The use of a global data set for calibration makes  
271 it possible to sample a large range of climates, and thus makes it more likely that the  
272 reconstructions of glacial climates are realistic and not confined to the limited climate range  
273 sampled in any one region (Turner et al., 2020). Indeed, Turner et al. (2020) have shown that  
274 increasing the size of the calibration data set tends to lead to smaller reconstruction errors and  
275 more accurate estimates of taxon coefficients. Pragmatically, the use of a global data set also  
276 facilitates making reconstructions for sites from regions where there is limited modern pollen  
277 data.~~

278 These reconstructions can be used as targets for model evaluation, specifically the two transient  
 279 D-O experiments planned for the next phase of the Palaeoclimate Modelling Intercomparison  
 280 (see Malmierca-Vallet et al., 2023 for the experimental protocol). The first of these experiments  
 281 is a baseline simulation starting at 34 ka, a time with low obliquity, moderate MIS3 greenhouse  
 282 gas values, and an intermediate ice sheet configuration, which appears to be most conducive to  
 283 generating D–O-like behaviour in climate models. The second experiment involves the  
 284 addition of freshwater, to examine whether this is necessary to precondition a state conducive  
 285 to generating D–O events. The observed anti-phasing in temperature changes between the  
 286 northern and southern hemispheres is a general feature of climate model experiments. Most  
 287 models show larger warming in winter than in summer in the northern hemisphere (e.g.  
 288 Flückiger et al., 2008; ~~Van Meersbeeck~~Van Meerbeeck et al., 2011; Izumi et al., 2023), which  
 289 is also consistent with our reconstructions. Models generally show an intensification of the  
 290 northern hemisphere monsoons during D-O events (e.g. Menviel et al., 2020; Izumi et al., 2023),  
 291 but there is less consistency about changes in plant-available moisture in the extratropics. Our  
 292 reconstructions of  $\alpha$  suggest an intensification of the northern hemisphere monsoons, consistent  
 293 with the simulations, and provide an opportunity to evaluate spatial patterns of moisture  
 294 changes over the extratropics. The reconstructions also indicate an increase in  $\alpha$  across much  
 295 of the tropics, including northern South America, West Africa and southern China and Japan  
 296 ([Figure 5](#)). Although  $\alpha$  is not a direct reflection of summer precipitation, these changes are  
 297 consistent with enhanced northern hemisphere monsoons during warming events, as shown by  
 298 speleothem records from the Caribbean (Warken et al., 2019) and speleothem and pollen records  
 299 from Asia (Wang et al., 2001; Zorzi et al., 2022; Fohlmeister et al., 2023). ~~Although there is~~  
 300 ~~some consistency in the broadscale patterns of changes in temperature and moisture across D-~~  
 301 ~~O events, the magnitude of the changes as well as the spatial patterning varies between events.~~

302 Identifying D-O events in pollen records is often problematic, particularly in regions where  
 303 warming (especially if accompanied by dryer conditions) leads to a reduction (or an hiatus) in  
 304 sedimentation as reflected in the variable resolution of the available pollen records (e.g.  
 305 Sinopoli et al., 2019; Wei et al., 2021; Camuera et al., 2022; Pini et al., 2022). The use of shorter  
 306 periods (Alshehri et al., 2019) goes some way to improving the identification of potential D-O  
 307 events using dynamic time warping (Alshehri et al., 2019). Thus, we were able to identify ~~D-~~  
 308 ~~O events only~~ 86% of the 348 individual D-O events that ~~occurred~~should occur during the  
 309 intervals covered by the 60 records available globally. It is also likely that some of the  
 310 variability in the reconstructed changes between different D-O events reflects imperfect

311 identification of specific events because of the comparatively modest resolution of the records.  
312 Several new high-resolution records covering MIS3 have become available since the  
313 compilation of the ACER database (e.g. Bird et al., 2024; Wei et al., 2021; Camuera et al.,  
314 2022; Pini et al., 2022; Rowe et al., 2024; Shichi et al., 2023; Zorzi et al., 2022) and including  
315 these newer records could help to improve the reliability of the global reconstructions presented  
316 here. ~~Nevertheless, this first compilation of quantitative climate reconstructions through~~  
317 ~~multiple D-O events during MIS3 provides an opportunity for evaluation of the transient D-O~~  
318 ~~simulations planned as part of the next phase of the Palaeoclimate Modelling Intercomparison~~  
319 ~~Project (Malmierca-Vallet et al., 2023).~~

320

321 **Data and code availability.** All the data used are public access and cited here. The code used  
322 to generate the reconstructions and figures is available at [https://github.com/ml4418/DO-](https://github.com/ml4418/DO-climate-reconstruction-paper.git)  
323 [climate-reconstruction-paper.git](https://github.com/ml4418/DO-climate-reconstruction-paper.git)

324 **Author contributions.** ML, SPH and ICP designed the study. ML made the reconstructions  
325 and produced the figures and tables. ML and SPH carried out the analyses. SPH wrote the first  
326 draft of the paper and all authors contributed to the final draft.

327 **Competing Interests.** The authors declare not competing interests.

328 **Acknowledgements.** ML acknowledges support from Imperial College through the Lee  
329 Family Scholarship. ICP acknowledges support from the ERC under the European Union  
330 Horizon 2020 research and innovation programme (grant agreement no.: 787203 REALM).  
331 SPH acknowledges fruitful discussions with colleagues from the D-O community working  
332 group.

333

## 334 **References**

335 Adolphi, F., Bronk Ramsey, C., Erhardt, T., Edwards, R. L., Cheng, H., Turney, C. S. M.,  
336 Cooper, A., Svensson, A., Rasmussen, S. O., Fischer, H., and Muscheler, R.:  
337 Connecting the Greenland ice-core and U / Th timescales via cosmogenic  
338 radionuclides: testing the synchronicity of Dansgaard–Oeschger events, *Clim. Past*, 14,  
339 1755–1781, <https://doi.org/10.5194/cp-14-1755-2018>, 2018.

- 340 Alshehri, M., Coenen, F., and Dures, K.: Effective sub-sequence-based dynamic time warping.  
341 In: Bramer, M., Petridis, M. (eds) Artificial Intelligence XXXVI. SGAI 2019. Lecture  
342 Notes in Computer Science, 11927. Springer, Cham. <https://doi.org/10.1007/978-3->  
343 [030-34885-4\\_23](https://doi.org/10.1007/978-3-030-34885-4_23), 2019.
- 344 Ampel, L., Bigler, C., Wohlfarth, B., Risberg, J., Lotter, A.F., and Veres, D.: Modest summer  
345 temperature variability during DO cycles in western Europe, *Quat. Sci. Rev.*, 29, 1322–  
346 1327, <https://doi.org/10.1016/j.quascirev.2010.03.002>, 2010.
- 347 Bauska, T. K., Marcott, S. A. and Brook, E. J.: Abrupt changes in the global carbon cycle  
348 during the last glacial period, *Nat. Geosci.*, 14(2), 91–96, doi:10.1038/s41561-020-  
349 00680-2, 2021.
- 350 Bellman, R., and Kalaba, R.: On adaptive control processes, *Automatic Control, IRE*  
351 *Transactions*, 4, 1–9, [http://ieeexplore.ieee.org/xpls/abs\\_all.jsp?arnumber=1104847](http://ieeexplore.ieee.org/xpls/abs_all.jsp?arnumber=1104847),  
352 1959.
- 353 Bird, M., Brand, M., Comley, R., Fu, X., Hadeen, X., Jacobs, Z., Rowe, C., Wurster, C., Zwart,  
354 C. and Bradshaw, C.: Late Pleistocene emergence of an anthropogenic fire regime in  
355 Australia’s tropical savannahs, *Nat. Geosci.*, 17, doi:10.1038/s41561-024-01388-3,  
356 2024.
- 357 Burstyn, Y., Gazit, A., and Omri Dvir, O.: Hierarchical Dynamic Time Warping methodology  
358 for aggregating multiple geological time series, *Comp. & Geosci.*, 150, 104704,  
359 <https://doi.org/10.1016/j.cageo.2021.104704>, 2021.
- 360 Camuera, J., Ramos-Román, M.J., Jiménez-Moreno, G. *et al.*: Past 200 kyr hydroclimate  
361 variability in the western Mediterranean and its connection to the African Humid  
362 Periods, *Sci. Rep.*, 12, 9050, <https://doi.org/10.1038/s41598-022-12047-1>, 2022.
- 363 Corrick, E.C., Drysdale, R.N., Hellstrom, J.C., Capron, E., Rasmussen, S.O., Zhang, X.,  
364 Fleitmann, D., Couchoud, I., and Wolff, E.: Synchronous timing of abrupt climate  
365 changes during the last glacial period, *Science*, 369, 963–969,  
366 <https://doi.org/10.1126/science.aay5538>, 2020.

- 367 Crisp, M. D. and Cook, L. G.: Phylogenetic niche conservatism: What are the underlying  
368 evolutionary and ecological causes?, *New Phytol.*, 196(3), 681–694,  
369 doi:10.1111/j.1469-8137.2012.04298.x, 2012.
- 370 Dansgaard, W., Johnsen, S.J., Clausen, H.B., Dahl-Jensen, D., Gundestrup, N.S., Hammer,  
371 C.U., Hvidberg, C.S., Steffensen, J.P., Sveinbjörnsdóttir, A.E., Jouzel, J., and Bond,  
372 G.: Evidence for general instability of past climate from a 250-kyr ice-core record,  
373 *Nature*, 364, 218–220, <https://doi.org/10.1038/364218a0>, 1993.
- 374 Denniston, R.F., Asmerom, Y., Polyak, V., Dorale, J.A., Carpenter, S.J., Trodick, C., Hoye,  
375 B., and González, L.A.: Synchronous millennial-scale climatic changes in the Great  
376 Basin and the North Atlantic during the last interglacial. *Geology* 35, 619-622, 2007.
- 377 Doblus-Reyes, F. J., Sörensson, A. A., Almazroui, M., Dosio, A., Gutowski, W. J., Haarsma,  
378 R., Hamdi, R., Hewitson, B., Kwon, W.-T., Lamptey, B. L., Maraun, D., Stephenson,  
379 T. S., Takayabu, I., Terray, L., Turner, A. and Zuo, Z.: Linking global to regional  
380 climate change, in *Climate Change 2021 – The Physical Science Basis: Working Group  
381 I Contribution to the Sixth Assessment Report of the Intergovernmental Panel on  
382 Climate Change*, edited by V. Masson-Delmotte, P.Zhai, A. Pirani, S. L. Connors, C.  
383 Péan, S. Berger, N. Caud, Y. Chen, L. Goldfarb, M. I. Gomis, M. Huang, K. Leitzell,  
384 E.Lonnoy, J. B. R. Matthews, T. K. Maycock, T. Waterfield, O. Yelekçi, R. Yu, and B.  
385 Zhou, pp. 1363–1512, Cambridge University Press, Cambridge, United Kingdom and  
386 New York, NY, USA., 2021.Fleitmann, D., Cheng, H., Badertscher, S., Edwards, R.L.,  
387 Mudelsee, M., Göktürk, O.M., Fankhauser, A., Pickering, R., Raible, C.C., Matter, A.,  
388 Kramers, J., and Tüysüz, O.: Timing and climatic impact of Greenland interstadials  
389 recorded in stalagmites from northern Turkey, *Geophys. Res. Lett.*, 36, 2009.
- 390 Fletcher, W.F., Sánchez Goñi, M.F., Allen, J.R.M., Cheddadi, R., Combourieu-Nebout, N.,  
391 Huntley, B., Lawson, I., Londeix, L., Magri, D., Margari, V., Müller, U.C., Naughton,  
392 F., Novenko, E., Roucoux, K., Tzedakis, P.C.: Millennial-scale variability during the  
393 last glacial in vegetation records from Europe, *Quat. Sci. Rev.*, 29, 2839-2864,  
394 <https://doi.org/10.1016/j.quascirev.2009.11.015>, 2010.

- 395 Flückiger, J., Knutti, R., White, J.W.C., and Renssen, H.: Modeled seasonality of glacial abrupt  
396 climate events, *Clim. Dyn.*, 31, 633–645, <https://doi.org/10.1007/s00382-008-0373-y>,  
397 2008.
- 398 Fohlmeister, J., Sekhon, N., Columbu, A., Vettoretti, G., Weitzel, N., Rehfeld, K., Veiga-Pires,  
399 C., Ben-Yami, M., Marwan, N. and Boers, N.: Global reorganization of atmospheric  
400 circulation during Dansgaard–Oeschger cycles, *Proc. Natl. Acad. Sci.*, 120(36),  
401 e2302283120, doi:10.1073/pnas.2302283120, 2023.
- 402 Grigg, L.D., and Whitlock, C.: Patterns and causes of millennial-scale climate change in the  
403 Pacific Northwest during Marine Isotope Stages 2 and 3, *Quat. Sci. Rev.*, 21, 2067-  
404 2083, 2002.
- 405 Grimm, E.C., Watts, W.A., Jacobson, G.L., Hansen, B.C.S., Almquist, H., and Dieffenbacher-  
406 Krall, A.C.: Evidence for warm wet Heinrich events in Florida, *Quat. Sci. Rev.*, 25,  
407 2197-2211, 2006.
- 408 Grygar, T., Kadlec, J., Pruner, P., Swann, G., Bezdicka, P., Hradil, D., Lang, K., Novotna, K.,  
409 and Oberhänsli, H.: Paleoenvironmental record in Lake Baikal sediments:  
410 environmental changes in the last 160 ky, *Palaeogeogr. Palaeoclimatol. Palaeoecol.*,  
411 237, 240-254, 2006.
- 412 Guiot, J., de Beaulieu, J. L., Cheddadi, R., David, F., Ponel, P., and Reille, M.: The climate in  
413 Western Europe during the last Glacial/Interglacial cycle derived from pollen and insect  
414 remains, *Palaeogeogr., Palaeoclimatol., Palaeoecol.*, 103, 73–93,  
415 [https://doi.org/10.1016/0031-0182\(93\)90053-L](https://doi.org/10.1016/0031-0182(93)90053-L), 1993.
- 416 Jiménez-Moreno, G., Anderson, R.S., Desprat, S., Grigg, L.D., Grimm, E.C., Heusser, L.E.,  
417 Jacobs, B.F., López-Martínez, C., Whitlock, C.L., and Willard, D.A.: Millennial-scale  
418 variability during the last glacial in vegetation records from North America, *Quat. Sci.*  
419 *Rev.*, 29, 2865-2881, <https://doi.org/10.1016/j.quascirev.2009.12.013>, 2010.
- 420 Harrison, S.P., and Sánchez Goñi, M.F.: Global patterns of vegetation response to millennial-  
421 scale variability during the last glacial: A synthesis. *Quat. Sci. Rev.*, 29, 2957-2980,  
422 2010.

- 423 Harvey, P. H. and Pagel, M. D.: The comparative method in evolutionary biology, Oxford  
424 University Press., 1991.
- 425 Huber, C., Leuenberger, M., Spahni, R., Flückiger, J., Schwander, J., Stocker, T.F., Johnsen,  
426 S., Landais, A., and Jouzel, J.: Isotope calibrated Greenland temperature record over  
427 Marine Iso- tope Stage 3 and its relation to CH<sub>4</sub>, *Earth Planet. Sci. Lett.*, 243, 504–519,  
428 2006.
- 429 Huntley, B., Bartlein, P. J. and Prentice, I. C.: Climatic control of the distribution and  
430 abundance of Beech (*Fagus L.*) in Europe and North America, *J. Biogeogr.*, 16(6), 551–  
431 560, doi:10.2307/2845210, 1989.
- 432 Huntley, B., Watts, W.A., Allen, J.R.M., Zolitschka, B.: Palaeoclimate, chronology and  
433 vegetation history of the Weichselian Lateglacial: comparative analysis of data from  
434 three cores at Lago Grande di Monticchio, southern Italy, *Quat. Sci. Rev.*, 18: 945-960,  
435 [https://doi.org/10.1016/S0277-3791\(99\)00007-4](https://doi.org/10.1016/S0277-3791(99)00007-4), 1999.
- 436 IPCC: Climate change 2022: Impacts, adaptation and vulnerability. Contribution of working  
437 group II to the sixth assessment report of the Intergovernmental Panel on Climate  
438 Change, edited by H.-O. Pörtner, D. C. Roberts, M. Tignor, E. S. Poloczanska, K.  
439 Mintenbeck, A. Alegría, M. Craig, S. Langsdorf, S. Löschke, V. Möller, A. Okem, and  
440 B. Rama, Cambridge University Press, Cambridge University Press, Cambridge, UK  
441 and New York, NY, USA., 2022.
- 442 Jiang, K., Wang, Q., Dimitrov, D., Luo, A., Xu, X., Su, X., Liu, Y., Li, Y., Li, Y. and Wang, Z.:  
443 Evolutionary history and global angiosperm species richness–climate relationships,  
444 *Glob. Ecol. Biogeogr.*, 32(7), 1059–1072, doi:10.1111/geb.13687, 2023.
- 445 Kindler, P., Guillevic, M., Baumgartner, M., Schwander, J., Landais, A., and Leuenberger, M.:  
446 Temperature reconstruction from 10 to 120 kyr b2k from the NGRIP ice core, *Clim.*  
447 *Past*, 10, 887–902, <https://doi.org/10.5194/cp-10-887-2014>, 2014.
- 448 Lee, J.-Y., Marotzke, J., Bala, G., Cao, L., Corti, S., Dunne, J. P., Engelbrecht, F., Fischer, E.,  
449 Fyfe, J. C., Jones, C., Maycock, A., Mutemi, J., Ndiaye, O., Panickal, S. and Zhou, T.:  
450 Future global climate: Scenario-based projections and near- term information, in  
451 *Climate change 2021: The physical science basis. Contribution of working group I to*

- 452 the sixth assessment report of the Intergovernmental Panel on Climate Change, edited  
453 by V. Masson-Delmotte, P. Zhai, A. Pirani, S. L. Connors, C. Péan, S. Berger, N. Caud,  
454 Y. Chen, L. Goldfarb, M. I. Gomis, M. Huang, K. Leitzell, E. Lonnoy, J. B. R.  
455 Matthews, T. K. Maycock, T. Waterfield, O. Yelekçi, R. Yu, and B. Zhou, pp. 553–672,  
456 Cambridge University Press, Cambridge, United Kingdom and New York, NY, USA.,  
457 2021.
- 458 Liu, M., Prentice, I.C., ter Braak, C.J.F, and Harrison, S.P.: An improved statistical approach  
459 for reconstructing past climates from biotic assemblages, *Proc. Royal Soc., Math. A*,  
460 476, 20200346, 20200346, <https://doi.org/10.1098/rspa.2020.0346>, 2020.
- 461 Liu, M., Shen, Y., González-Sampériz, P., Gil-Romera, G., ter Braak, C.J.F. Prentice, I.C., and  
462 Harrison, S.P.: Holocene climates of the Iberian Peninsula, *Clim. Past* 19, 803-834,  
463 <https://doi.org/10.5194/cp-19-803-2023>, 2023.
- 464 Malmierca-Vallet, I., Sime, L.C., and the D–O community members: Dansgaard–Oeschger  
465 events in climate models: review and baseline Marine Isotope Stage 3 (MIS3) protocol,  
466 *Clim. Past*, 19, 915–942, <https://doi.org/10.5194/cp-19-915-2023>, 2023.
- 467 Menviel, L., Timmermann, A., Friedrich, T., and England, M. H.: Hindcasting the continuum  
468 of Dansgaard–Oeschger variability: mechanisms, patterns and timing, *Clim. Past* 10,  
469 63–77, 2014.
- 470 Menviel, L.C., Skinner, L.C., Tarasov, L., and Tzedakis, P.C.: An ice–climate oscillatory  
471 framework for Dansgaard–Oeschger cycles, *Nat. Rev. Earth Environ.*, 1, 677–693,  
472 <https://doi.org/10.1038/s43017-020-00106-y>, 2020.
- 473 Peterson, A. T.: Ecological niche conservatism: A time-structured review of evidence, *J.*  
474 *Biogeogr.*, 38(5), 817–827, doi:10.1111/j.1365-2699.2010.02456.x, 2011.
- 475 Pini, R., Furlanetto, G., Vallé, F., Badino, F., Wick, L., Anselmetti, F.S., Bertuletti, P., Fusi, N.,  
476 Morlock, M.A., Delmonte, B., Harrison, S.P., Maggi, V., Ravazzi, C.: Linking North  
477 Atlantic and Alpine Last Glacial Maximum climates via a high-resolution pollen-based  
478 subarctic forest steppe record, *Quat. Sci. Rev.*, 294, 107759,  
479 <https://doi.org/10.1016/j.quascirev.2022.107759>, 2022.

- 480 [Prentice, I. C., Cleator, S. F., Huang, Y. H., Harrison, S. P. and Roulstone, I.: Reconstructing](#)  
481 [ice-age palaeoclimates: Quantifying low-CO<sub>2</sub> effects on plants, \*Glob. Planet. Change,\*](#)  
482 [149, 166–176, doi:<https://doi.org/10.1016/j.gloplacha.2016.12.012>, 2017.](#)
- 483 Prentice, I. C., Villegas-Diaz, R. and Harrison, S. P.: Accounting for atmospheric carbon  
484 dioxide variations in pollen-based reconstruction of past hydroclimates, *Glob. Planet.*  
485 *Change*, 211, 103790, doi:10.1016/j.gloplacha.2022.103790, 2022.
- 486 Prud'homme, C., Fischer, P., Jöris, O., Gromov, S., Vinnepand, M., Hatté, C., Vonhof, H.,  
487 Moine, O., Vött, A., and Fitzsimmons, K. E.: Millennial-timescale quantitative  
488 estimates of climate dynamics in central Europe from earthworm calcite granules in  
489 loess deposits, *Commun. Earth Environ.*, 3, 1–14, [https://doi.org/10.1038/s43247-022-](https://doi.org/10.1038/s43247-022-00595-3)  
490 [00595-3](https://doi.org/10.1038/s43247-022-00595-3), 2022.
- 491 Rowe, C., Brand, M., Wurster, C. M. and Bird, M. I.: Vegetation changes through stadial and  
492 interstadial stages of MIS 4 and MIS 3 based on a palynological analysis of the  
493 Girraween Lagoon sediments of Darwin, Australia, *Palaeogeogr. Palaeoclimatol.*  
494 *Palaeoecol.*, 642, 112150, doi:10.1016/j.palaeo.2024.112150, 2024.
- 495 Sánchez Goñi, M., Cacho, I., Turon, J., Guiot, J., Sierro, F., Peyrouquet, J., Grimalt, J. and  
496 Shackleton, N.: Synchronicity between marine and terrestrial responses to millennial  
497 scale climatic variability during the last glacial period in the Mediterranean region,  
498 *Clim. Dyn.*, 19(1), 95–105, doi:10.1007/s00382-001-0212-x, 2002.
- 499 Sánchez Goñi, M.F., and Harrison, S.P.: Millennial-scale climate variability and vegetation  
500 changes during the Last Glacial: Concepts and terminology, *Quat. Sci. Rev.*, 29, 2823–  
501 2827, 2010.
- 502 Sánchez Goñi, M.F., Desprat, S., Daniau, A.-L., Bassinot, F., Polanco-Martínez, J.M., Harrison,  
503 S.P., Allen, J.R.P., Anderson, R.S., Behling, H., Bonnefille, R., Burjachs, F., Carrión,  
504 J.S., Cheddadi, R., Clark, J.S., Combourieu-Nebout, N., Courtney-Mustaphi, C.,  
505 Debusk, G.H., Dupont, L.M., Finch, J., Fletcher, W.J., Giardini, M., González, C.,  
506 Gosling, W.D., Grigg, L.D., Grimm, E.C., Hayashi, R., Helmens, K., Heusser, L.E.,  
507 Hill, T., Hope, G., Huntley, B., Igarashi, Y., Irino, T., Jacobs, B.F., Jiménez-Moreno, G.,  
508 Kawai, S., Kershaw, P., Kumon, F., Lawson, I., Ledru, M.-P., Lézine, A.-M., Liew, P.-  
509 M., Magri, D., Marchant, R., Margari, V., Mayle, F., McKenzie, M., Moss, P., Müller,

- 510 S., Müller, U.C., Naughton, F., Newnham, R.M., Oba, T., Pérez-Obiol, R., Pini, R.,  
511 Ravazzi, C., Roucoux, K.H., Rucina, S., Scott, L., Takahara, H., Tzedakis, P.C., Urrego,  
512 D.H., Van Geel, B., Valencia, B.G., Vandergoes, M.J., Vincens, A., Whitlock, C.L.,  
513 Willard, D. A., and Yamamoto, M.: The ACER pollen and charcoal database: a global  
514 resource to document vegetation and fire response to abrupt climate changes of the last  
515 glacial period, *Earth Syst. Sci. Data* 9: 679-695, 2017.
- 516 Shichi, K., Goebel, T., Izuho, M. and Kashiwaya, K.: Climate amelioration, abrupt vegetation  
517 recovery, and the dispersal of *Homo sapiens* in Baikal Siberia, *Sci. Adv.*, 9(38),  
518 eadi0189, doi:10.1126/sciadv.adi0189, 2024.
- 519 Sinopoli, G., Peyron, O., Masi, A., Holtvoeth, J., Francke, A., Wagner, B., and Sadori, L.:  
520 Pollen-based temperature and precipitation changes in the Ohrid Basin (western  
521 Balkans) between 160 and 70 ka, *Clim. Past*, 15, 53–71, [https://doi.org/10.5194/cp-15-](https://doi.org/10.5194/cp-15-53-2019)  
522 53-2019, 2019.
- 523 Stockhecke, M., Timmermann, A., Kipfer, R., Haug, G.H., Kwiecien, O., Friedrich, T.,  
524 Menviel, L., Litt, T., Pickarski, N., and Anselmetti, F.S.: Millennial to orbital-scale  
525 variations of drought intensity in the Eastern Mediterranean, *Quat. Sci. Rev.*, 133, 77-  
526 95, 2016.
- 527 Turner, M. G., Wei, D., Prentice, I. C. and Harrison, S. P.: The impact of methodological  
528 decisions on climate reconstructions using WA-PLS, *Quat. Res.*, 99, 341–356,  
529 doi:10.1017/qua.2020.44, 2021.
- 530 Újvári, G., Bernasconi, S. M., Stevens, T., Kele, S., Páll-Gergely, B., Surányi, G., and Demény,  
531 A.: Stadial-Interstadial Temperature and Aridity Variations in East Central Europe  
532 Preceding the Last Glacial Maximum, *Paleoceanog. Paleoclim.*, 36, e2020PA004170,  
533 <https://doi.org/10.1029/2020PA004170>, 2021.
- 534 Van Meerbeeck, C.J., Renssen, H., Roche, D.M., Wohlfarth, B., Bohncke, S.J.P., Bos, J.A.A.,  
535 Engels, S., Helmens, K.F., Sánchez-Goñi, M.F., Svensson, A., and Vandenberghe, J.:  
536 The nature of MIS 3 stadial-interstadial transitions in Europe: New insights from  
537 model-data comparisons, *Quat. Sci. Rev.*, 30, 3618–3637,  
538 <https://doi.org/10.1016/j.quascirev.2011.08.002>, 2011.

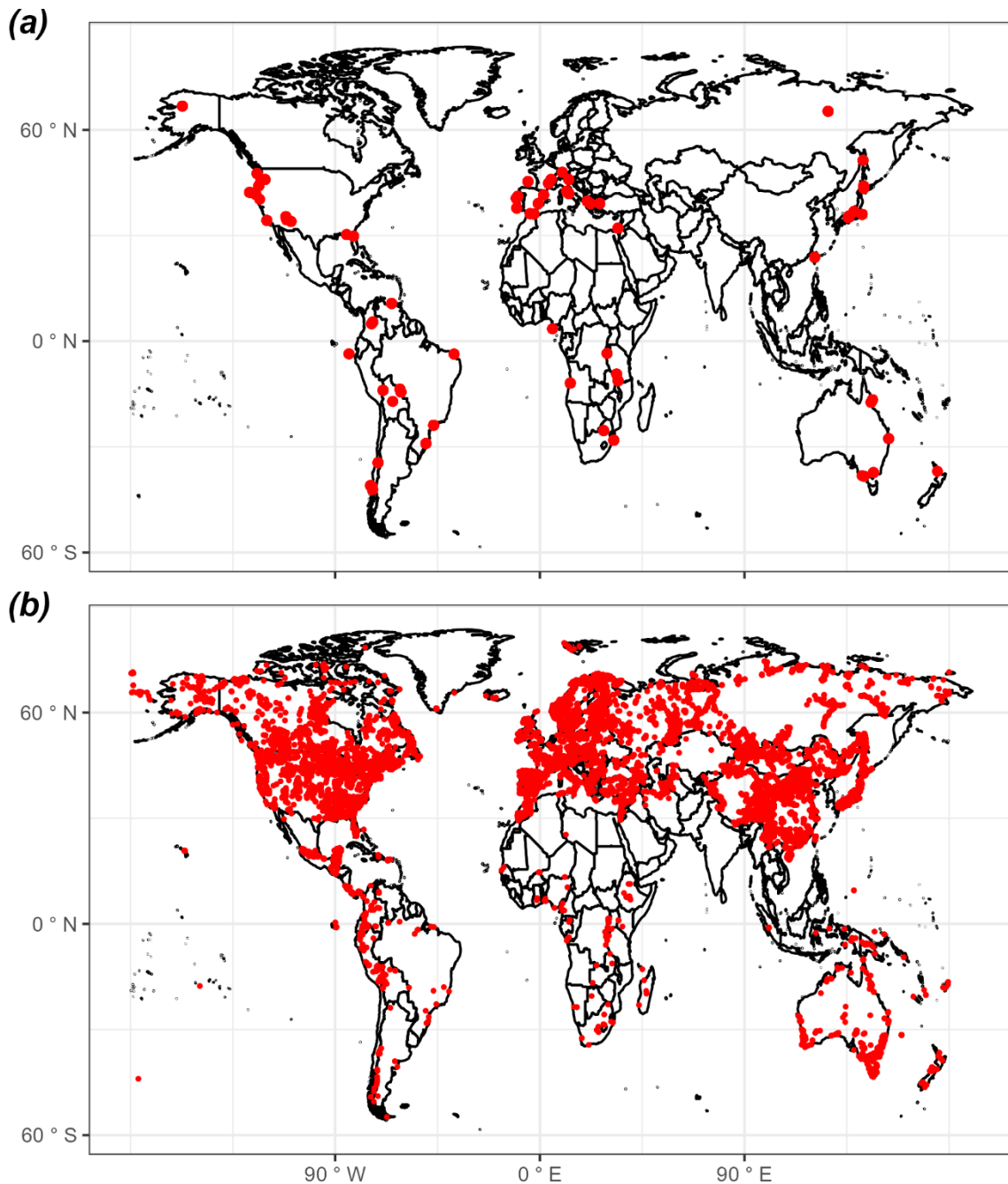
- 539 Villegas-Diaz, R., and Harrison, S.P.: The SPECIAL Modern Pollen Data Set for Climate  
540 Reconstructions, version 2 (SMPDSv2). University of Reading.  
541 Dataset. <https://doi.org/10.17864/1947.000389>, 2022.
- 542 Voelker, A.H.: Global distribution of centennial-scale records for Marine Isotope Stage (MIS)  
543 3: a database, *Quat. Sci. Rev.*, 21, 1185–1212, 2002.
- 544 Wang, Y. J., Cheng, H., Edwards, R. L., An, Z. S., Wu, J. Y., Shen, C.-C. and Dorale, J. A.: A  
545 high-resolution absolute-dated Late Pleistocene monsoon record from Hulu Cave,  
546 China, *Science* (80-. ), 294(5550), 2345–2348, doi:10.1126/science.1064618, 2001.
- 547 Warken, S. F., Scholz, D., Spötl, C., Jochum, K. P., Pajón, J. M., Bahr, A. and Mangini, A.:  
548 Caribbean hydroclimate and vegetation history across the last glacial period, *Quat. Sci.*  
549 *Rev.*, 218, 75–90, doi:10.1016/j.quascirev.2019.06.019, 2019.
- 550 Wei, D., González-Sampériz, P., Gil-Romera, G., Harrison, S.P., and Prentice, I.C.: Seasonal  
551 temperature and moisture changes in interior semi-arid Spain from the last interglacial  
552 to the Late Holocene, *Quat. Res.*, 101, 143–155, <https://doi.org/10.1017/qua.2020.108>,  
553 2021.
- 554 Wiens, J. and Graham, C.: Niche conservatism: Integrating evolution, ecology, and  
555 conservation biology, *Annu. Rev. Ecol. Evol. Syst.*, 36, 519–539,  
556 doi:10.1146/annurev.ecolsys.36.102803.095431, 2005.
- 557 Wolff, E. W., Chappellaz, J., Blunier, T., Rasmussen, S. O. and Svensson, A.: Millennial-scale  
558 variability during the last glacial: The ice core record, *Quat. Sci. Rev.*, 29(21), 2828–  
559 2838, doi:10.1016/j.quascirev.2009.10.013, 2010.
- 560 Yin, X., Jarvie, S., Guo, W.-Y., Deng, T., Mao, L., Zhang, M., Chu, C., Qian, H., Svenning, J.-  
561 C. and He, F.: Niche overlap and divergence times support niche conservatism in  
562 eastern Asia–eastern North America disjunct plants, *Glob. Ecol. Biogeogr.*, 30(10),  
563 1990–2003, doi:10.1111/geb.13360, 2021.
- 564 Zander, P. D., Böhl, D., Sirocko, F., Auderset, A., Haug, G. H. and Martínez-García, A.:  
565 Reconstruction of warm-season temperatures in central Europe during the past 60 000  
566 years from lacustrine branched glycerol dialkyl glycerol tetraethers (brGDGTs), *Clim.*  
567 *Past*, 20(4), 841–864, doi:10.5194/cp-20-841-2024, 2024.

568 Zorzi, C., Desprat, S., Clément, C., Thirumalai, K., Oliviera, D., Anupama, K., Prasad, S. and  
569 Martinez, P.: When eastern India oscillated between desert versus savannah-dominated  
570 vegetation, *Geophys. Res. Lett.*, 49(16), e2022GL099417,  
571 doi:10.1029/2022GL099417, 2022.

572

573 **Figures and Tables**

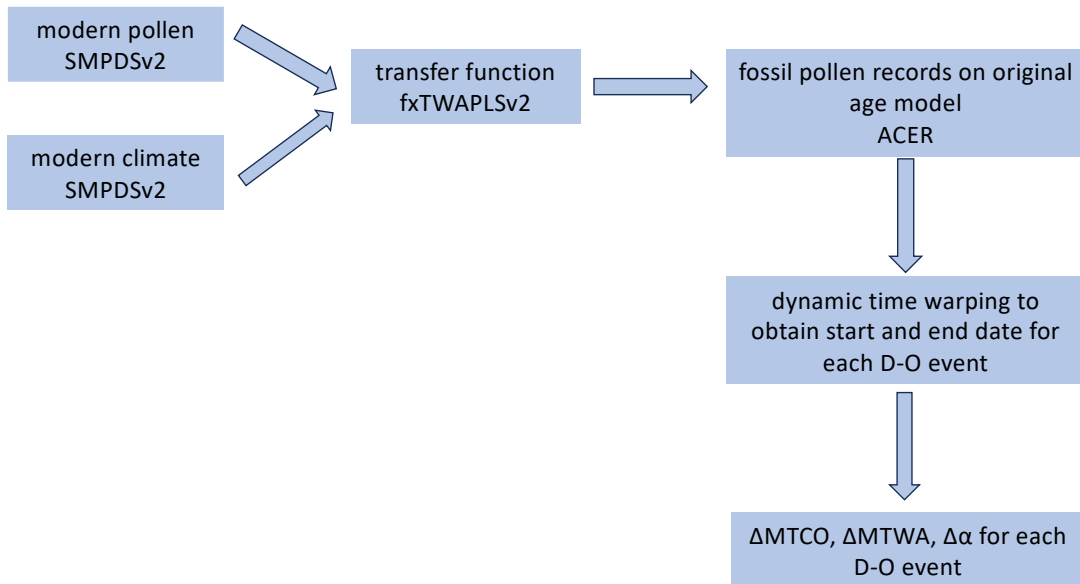
574 Figure 1: Map showing the locations of sites (a) from the Abrupt Climate Changes and  
575 Environmental Responses (ACER) database (Sánchez Goñi et al., 2017) covering the interval  
576 between 50 ka and 30 ka used for the reconstructions and (b) sites in version 2 of the SPECIAL  
577 Modern Pollen Data Set (SMPDSv2: Villegas-Diaz and Harrison, 2022) used to derive the  
578 transfer functions for these climate reconstructions.



579

580

581 Figure 2: Flow chart showing the reconstruction methodology.



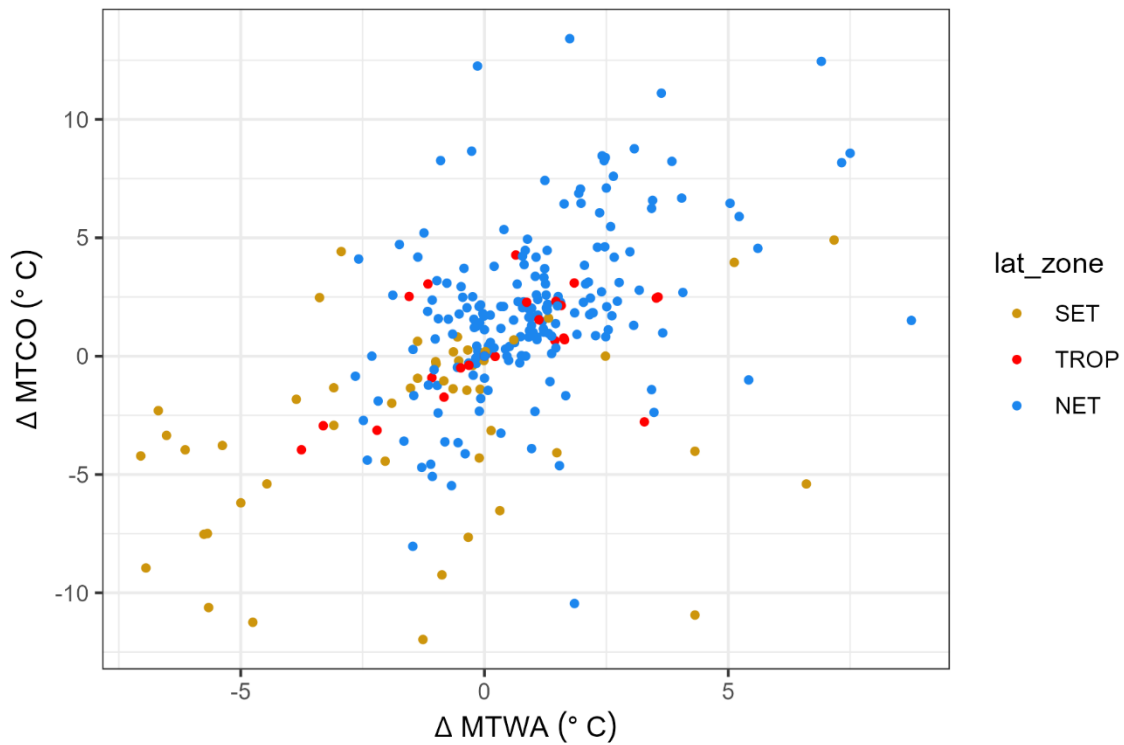
582

583

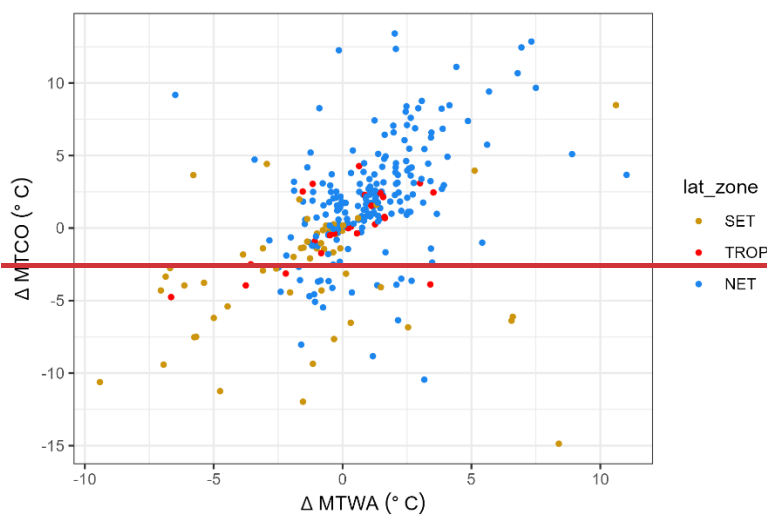
584

585

586 Figure 3: Scatter plot of the change in mean temperature of the coldest month ( $\Delta\text{MTCO}$ ) versus  
587 the change in mean temperature of the warmest month ( $\Delta\text{MTWA}$ ) during individual  
588 Dansgaard-Oeschger (D-O) events at individual sites. The points are colour-coded to indicate  
589 whether the sites are from the northern extratropics (NET, north of  $23.5^\circ\text{N}$ ), the tropics (TROP,  
590 between  $23.5^\circ\text{N}$  and  $23.5^\circ\text{S}$ ) or southern extratropics (SET, south of  $23.5^\circ\text{S}$ ).



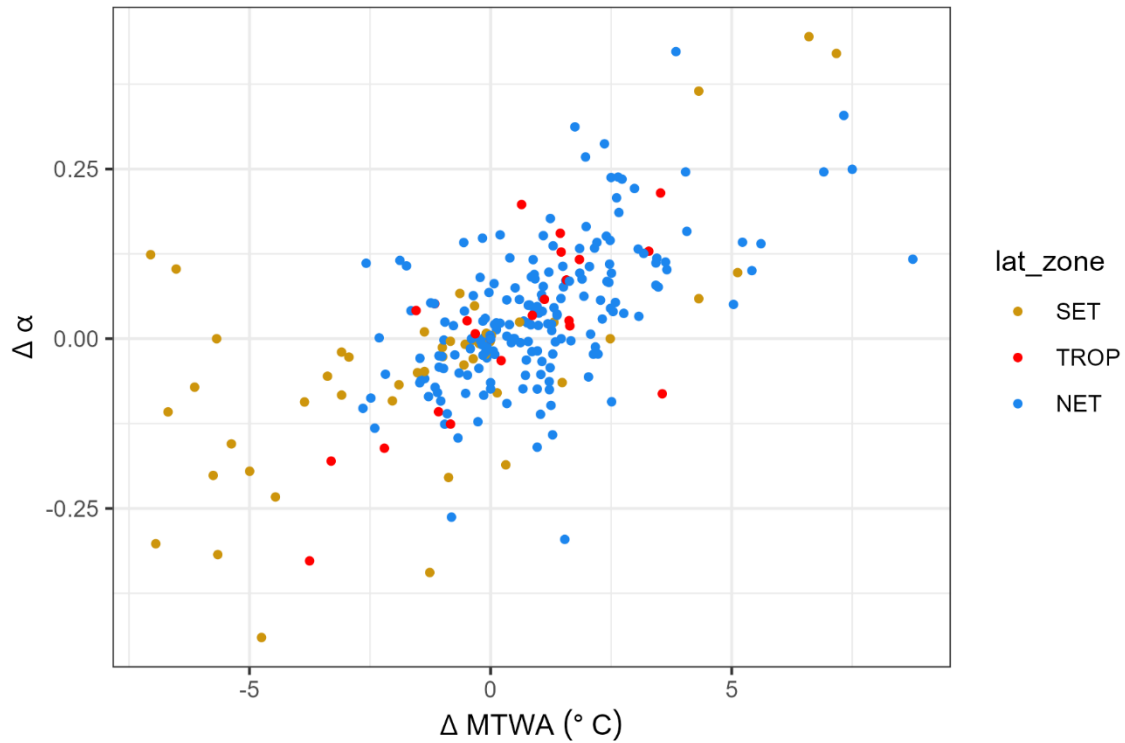
591



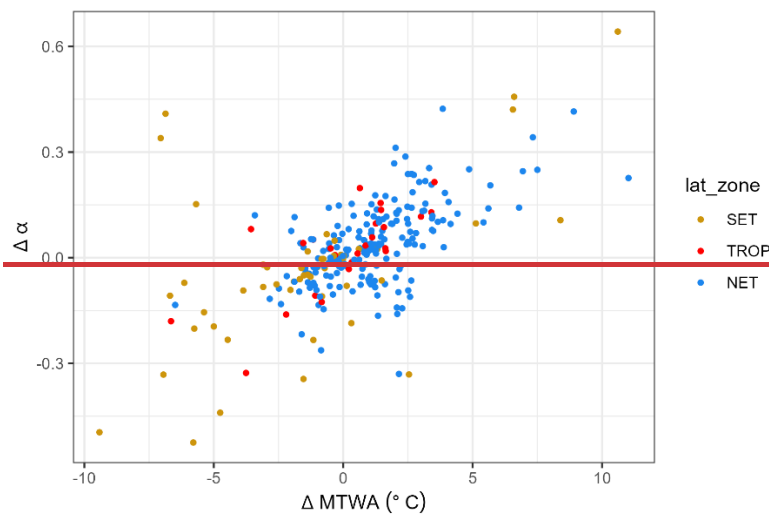
592

593

594 Figure 4: Scatter plot of the change in plant-available moisture ( $\Delta\alpha$ ) versus the change in mean  
595 temperature of the warmest month ( $\Delta\text{MTWA}$ ) during individual Dansgaard-Oeschger (D-O)  
596 events at individual sites. The points are colour-coded to indicate whether the sites are from  
597 the northern extratropics (NET, north of  $23.5^\circ\text{N}$ ), the tropics (TROP, between  $23.5^\circ\text{N}$  and  
598  $23.5^\circ\text{S}$ ) or southern extratropics (SET, south of  $23.5^\circ\text{S}$ ).



599

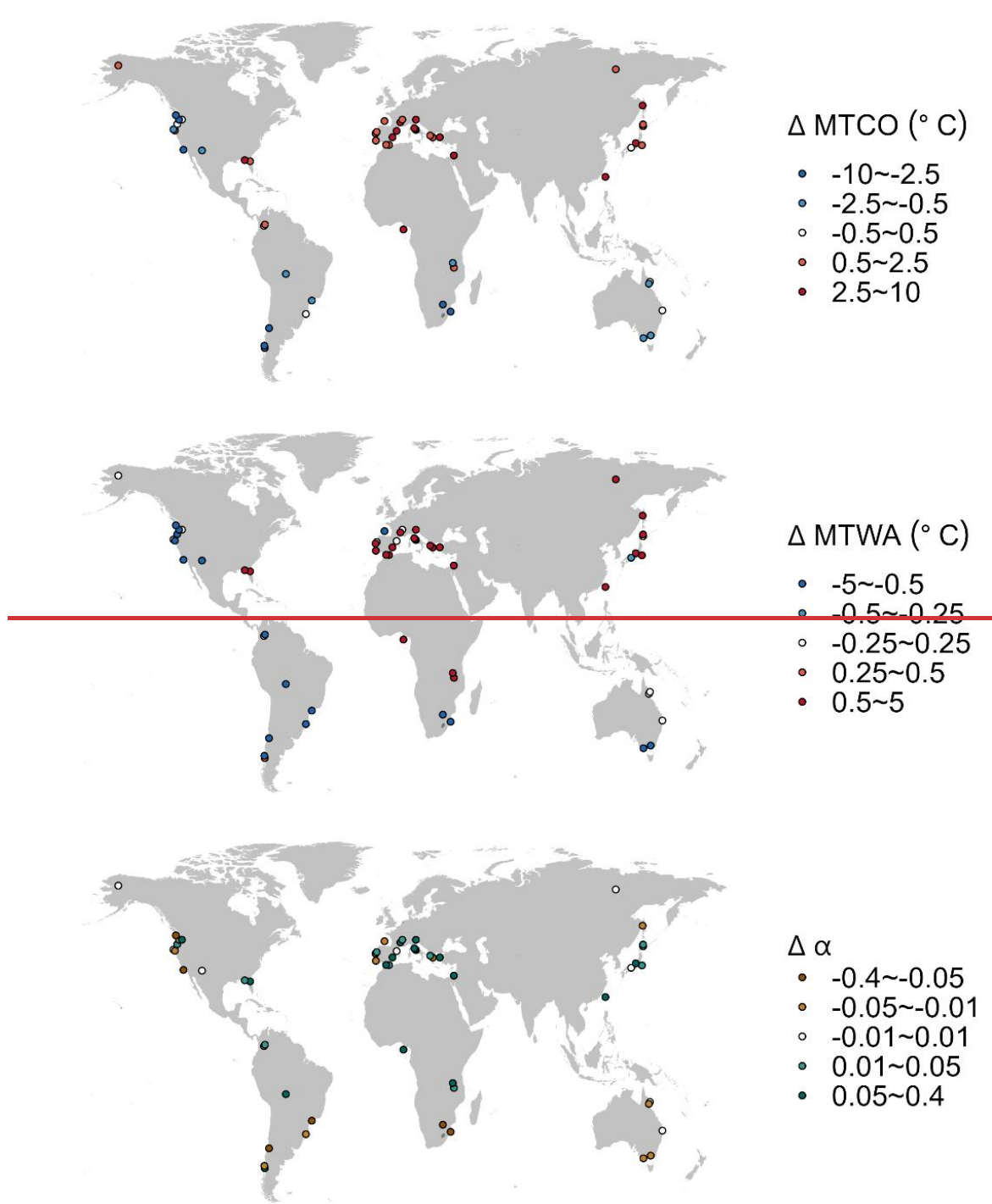


600

601

602 Figure 5: Maps showing the median change of site-based reconstructions for Dansgaard-  
603 Oeschger (D-O) events.





605

606

607 Table 1: Details of the sites from the Abrupt Climate Changes and Environmental Responses  
 608 (ACER) database (Sánchez Goñi et al., 2017) covering the interval between 50 ka and 30 ka  
 609 used for the climate reconstructions.  $n_{\text{due}}$  is the number of D-O events that should be found  
 610 based on the time interval covered by the record.  $n_{\text{miss}}$  is the number of D-O events that were  
 611 not identified.  $n_{\text{low}}$  is the number of D-O events missed because of low resolution of part of the  
 612 record. Some of the 73 sites (indicated by NA in  $n_{\text{due}}$ ,  $n_{\text{miss}}$  and  $n_{\text{low}}$ ) provide records for parts  
 613 of the 50-30ka interval but not for the intervals of the D-O events. Reconstructions based on  
 614 samples where the D-O signal was not identified were not used in subsequent analyses. The  
 615 full citations for each site are given in Supplementary Information.

| Site name              | Latitude | Longitude | Elevation (m) | Site type | Reference(s)   | $n_{\text{due}}$ | $n_{\text{miss}}$ | $n_{\text{low}}$ |
|------------------------|----------|-----------|---------------|-----------|--|------------------|-------------------|------------------|
| Abric Romani           | 41.53    | 1.68      | 350           | TERR      | <del>Burjachs &amp; Ramon (1994)</del> Burjachs & Julià (1994)               | <del>22</del>    | <del>00</del>     | <del>00</del>    |
| Azzano Decimo          | 45.8833  | 12.7165   | 10            | TERR      | Pini et al. (2009)   | <del>66</del>    | <del>22</del>     | <del>22</del>    |
| Caledonia Fen          | -37.3333 | 146.7333  | 1280          | TERR      | Kershaw et al. (2007b)   | <del>88</del>    | <del>12</del>     | <del>12</del>    |
| Cambara do Sul         | -29.05   | -50.1     | 1040          | TERR      | Behling et al. (2004)  | <del>77</del>    | <del>10</del>     | <del>00</del>    |
| Camel Lake             | 30.26    | -85.01    | 20            | TERR      | Watts et al. (1992)  | <del>22</del>    | <del>04</del>     | <del>04</del>    |
| Carp Lake              | 45.91    | -120.88   | 720           | TERR      | Whitlock and Bartlein (1997);<br>Whitlock et al. (2000)                      | <del>88</del>    | <del>14</del>     | <del>14</del>    |
| Colônia                | -23.87   | -46.71    | 900           | TERR      | Ledru et al. (2009)  | <del>77</del>    | <del>44</del>     | <del>44</del>    |
| Core Trident 163 31B   | -3.61    | -83.96    | -3210         | MARI      | Heusser and Shackleton (1994)  | <u>NA</u>        | <u>NA</u>         | <u>NA</u>        |
| Fargher Lake           | 45.88    | -122.58   | 200           | TERR      | Grigg and Whitlock (2002)  | <del>88</del>    | <del>14</del>     | <del>04</del>    |
| Fundo Nueva            | -41.28   | -73.83    | 66            | TERR      | Heusser et al. (2000)  | <del>66</del>    | <del>14</del>     | <del>00</del>    |
| Fuquene                | 5.45     | -73.46    | 2540          | TERR      | van Geel and van der Hammen (1973);<br>Mommersteeg (1998)                    | <del>77</del>    | <del>32</del>     | <del>32</del>    |
| Füramoos               | 47.98    | 9.88      | 662           | TERR      | Müller et al. (2003)   | <u>NA</u>        | <u>NA</u>         | <u>NA</u>        |
| GeoB3104               | -3.67    | -37.72    | -767          | MARI      | Behling et al. (2000)  | <u>NA</u>        | <u>NA</u>         | <u>NA</u>        |
| Hay Lake               | 34       | -109.425  | 2780          | TERR      | Jacobs (1985)  | <del>55</del>    | <del>34</del>     | <del>34</del>    |
| Ioannina               | 39.75    | 20.85     | 470           | TERR      | Tzedakis et al. (2002);<br>Tzedakis et al. (2004)                            | <del>88</del>    | <del>04</del>     | <del>00</del>    |
| Joe Lake               | 66.76667 | -157.217  | 183           | TERR      | Anderson (1988);<br>Anderson et al. (1994)                                   | <del>77</del>    | <del>33</del>     | <del>33</del>    |
| Kalaloch               | 47.6053  | -124.371  | 19            | TERR      | Heusser (1972)   | <del>88</del>    | <del>12</del>     | <del>00</del>    |
| Kamiyoshi Basin (KY01) | 35.102   | 135.586   | 335           | TERR      | Takahara et al. (2000);;<br>Takahara et al. (2007);<br>Hayashi et al. (2009) | <del>14</del>    | <del>00</del>     | <del>00</del>    |
| Kashiru Bog            | -3.47    | 29.57     | 2240          | TERR      | Bonnefille & Riollet (1988); Bonnefille et al. (1992)                        | <del>22</del>    | <del>12</del>     | <del>12</del>    |
| Kenbuchi Basin         | 44.05    | 142.383   | 135           | TERR      | Igarashi et al. (1993);<br>Igarashi (1996)                                   | <del>33</del>    | <del>00</del>     | <del>00</del>    |
| Khoe                   | 51.341   | 142.14    | 15            | TERR      | Igarashi et al. (2002)   | <del>66</del>    | <del>24</del>     | <del>24</del>    |
| Kohuora                | -36.95   | 174.8667  | 5             | TERR      | Newnham et al. (2007)  | <u>NA</u>        | <u>NA</u>         | <u>NA</u>        |

|                         |          |          |       |      |   |               |               |               |
|-------------------------|----------|----------|-------|------|---|---------------|---------------|---------------|
| Kurota Lowland          | 35.517   | 135.879  | 20    | TERR | Takahara & Kitagawa (2000)  | <del>NA</del> | <del>NA</del> | <del>NA</del> |
| KW31                    | 3.52     | 5.57     | -1181 | MARI | Lézine & Cazet (2005); Lézine et al. (2005)   | <del>22</del> | <del>00</del> | <del>00</del> |
| La Laguna               | 4.92     | -74.03   | 2900  | TERR | Helmens et al., 1(1996)   | <del>22</del> | <del>00</del> | <del>00</del> |
| Lac du Bouchet          | 44.83    | 3.82     | 1200  | TERR | Reille and de Beaulieu (1990)   | <del>88</del> | <del>00</del> | <del>00</del> |
| Lagaccione              | 42.57    | 11.8     | 355   | TERR | Magri (1999); Magri (2008)  | <del>77</del> | <del>02</del> | <del>02</del> |
| Laguna Bella Vista      | -13.6167 | -61.55   | 600   | TERR | Burbridge et al. (2004)   | <del>22</del> | <del>04</del> | <del>04</del> |
| Laguna Chaplin          | -14.4667 | -61.0667 | 600   | TERR | Burbridge et al. (2004)   | <del>14</del> | <del>04</del> | <del>04</del> |
| Lake Billyakh           | 65.2833  | 126.7833 | 340   | TERR | Müller et al. (2010)  | <del>44</del> | <del>00</del> | <del>00</del> |
| Lake Biwa (BIW95-4)     | 35.245   | 136.054  | 84    | TERR | Takemura et al. (2000); Hayashida et al. (2007); Hayashi et al. (2010)  | <del>NA</del> | <del>NA</del> | <del>NA</del> |
| Lake Consuelo (CON1)    | -13.95   | -68.991  | 1360  | TERR | Urrego et al. (2005); Urrego et al. (2010)  | <del>14</del> | <del>04</del> | <del>04</del> |
| Lake Malawi             | -11.22   | 34.42    | 470   | TERR | DeBusk (1998)   | <del>66</del> | <del>23</del> | <del>23</del> |
| Lake Masoko             | -9.33    | 33.75    | 840   | TERR | Vincens et al. (2007)   | <del>22</del> | <del>00</del> | <del>00</del> |
| Lake Nojiri             | 36.831   | 138.216  | 657   | TERR | Kumon et al. (2009)   | <del>88</del> | <del>00</del> | <del>00</del> |
| Lake Tulane             | 29.83    | -81.95   | 36    | TERR | Grimm et al. (1993); Grimm et al. (2006)  | <del>88</del> | <del>24</del> | <del>24</del> |
| Lake Wangoom LW87 core  | -38.35   | 142.6    | 100   | TERR | Harle et al. (2002)   | <del>77</del> | <del>24</del> | <del>24</del> |
| Lake Xinias             | 39.05    | 22.27    | 500   | TERR | Bottema (1979)  | <del>88</del> | <del>13</del> | <del>13</del> |
| Les Echets G            | 45.9     | 4.93     | 267   | TERR | de Beaulieu & Reille (1984)   | <del>88</del> | <del>00</del> | <del>00</del> |
| Little Lake             | 44.16    | -123.58  | 217   | TERR | Grigg et al. (2001)   | <del>55</del> | <del>00</del> | <del>00</del> |
| Lynchs Crater           | -17.3667 | 145.7    | 760   | TERR | Kershaw et al. (2007a)  | <del>88</del> | <del>12</del> | <del>12</del> |
| MD01-2421               | 36.02    | 141.77   | -2224 | MARI | Igarashi & Oba (2006); Oba et al. (2006); Aoki et al. (2008)  | <del>77</del> | <del>12</del> | <del>00</del> |
| MD03-2622 Cariaco Basin | 10.7061  | -65.1691 | -877  | MARI | González et al. (2008); González and Dupont (2009)  | <del>NA</del> | <del>NA</del> | <del>NA</del> |
| MD04-2845               | 45.35    | -5.22    | -4100 | MARI | Sánchez Goñi et al. (2008); Daniau et al. (2009)  | <del>88</del> | <del>02</del> | <del>02</del> |
| MD84-629                | 32.07    | 34.35    | -745  | MARI | Cheddadi & Rossignol-Strick (1995)  | <del>88</del> | <del>14</del> | <del>14</del> |
| MD95-2039               | 40.58    | -10.35   | -3381 | MARI | Roucoux et al. (2001); Roucoux et al. (2005)  | <del>88</del> | <del>00</del> | <del>00</del> |
| MD95-2042               | 37.8     | -10.17   | -3148 | MARI | Sánchez Goñi et al. (1999); Sánchez Goñi et al. (2000); Daniau et al. (2007); Sánchez Goñi et al. (2008); (Sánchez Goñi et al. (2009) | <del>88</del> | <del>00</del> | <del>00</del> |
| MD95-2043               | 36.14    | -2.621   | -1841 | MARI | Sánchez Goñi et al. (2002); Fletcher and Sánchez Goñi (2008)  | <del>88</del> | <del>10</del> | <del>10</del> |
| MD99-2331               | 41.15    | -9.68    | -2110 | MARI | Sánchez Goñi et al. (2005); Naughton et al. (2007); Sánchez Goñi et al. (2008); Naughton et al. (2009)                                | <del>88</del> | <del>14</del> | <del>14</del> |
| Megali Limni            | 39.1025  | 26.3208  | 323   | TERR | Margari et al. (2007); Margari et al. (2009)  | <del>66</del> | <del>04</del> | <del>00</del> |

|                          |          |          |       |      |   |               |               |               |
|--------------------------|----------|----------|-------|------|---|---------------|---------------|---------------|
| Mfabeni Peatland         | -28.1487 | 32.51867 | 11    | TERR | Finch & Hill (2008)   | <del>55</del> | <del>04</del> | <del>04</del> |
| Nakafurano               | 43.367   | 142.433  | 173   | TERR | Igarashi et al. (1993)  | <del>22</del> | <del>00</del> | <del>00</del> |
| Native Companion Lagoon  | -27.68   | 153.41   | 20    | TERR | Petherick et al. (2008a); Petherick et al. (2008b)  | <del>66</del> | <del>04</del> | <del>04</del> |
| Navarrés                 | 39.1     | -0.68    | 225   | TERR | Carrión & van Geel (1999)   | <del>33</del> | <del>04</del> | <del>00</del> |
| ODP 1233 C               | -41      | -74.45   | -838  | MARI | Lamy et al. (2004); Heusser et al. (2006)   | <del>NA</del> | <del>NA</del> | <del>NA</del> |
| ODP 820                  | -16.63   | 146.3    | -280  | MARI | Moss & Kershaw (2000); Moss & Kershaw (2007)  | <del>77</del> | <del>43</del> | <del>43</del> |
| ODP site 976             | 36.2     | -4.3     | -1108 | MARI | Nebout et al. (2002); Masson-Delmotte et al. (2005)   | <del>88</del> | <del>14</del> | <del>00</del> |
| ODP1019                  | 41.66    | -124.91  | 989   | MARI | Mix et al. (1999); Pisias et al. (2001)   | <del>88</del> | <del>12</del> | <del>12</del> |
| ODP1078C                 | -11.92   | 13.4     | -426  | MARI | Dupont & Behling (2006); Dupont et al. (2008)   | <del>NA</del> | <del>NA</del> | <del>NA</del> |
| ODP893A                  | 34.28    | -120.03  | -577  | MARI | Heusser (1998); Heusser (2000)  | <del>88</del> | <del>10</del> | <del>10</del> |
| Potato Lake              | 34.45    | -111.33  | 2222  | TERR | Anderson (1993)   | <del>44</del> | <del>24</del> | <del>24</del> |
| Rice Lake (Rice Lake 81) | 40.3     | -123.22  | 1100  | TERR | L. Heusser, unpublished data  | <del>NA</del> | <del>NA</del> | <del>NA</del> |
| Siberia                  | -17.09   | -64.72   | 2920  | TERR | Mourguiart & Ledru (2003)   | <del>14</del> | <del>14</del> | <del>14</del> |
| Stracciacappa            | 42.13    | 12.32    | 220   | TERR | Giardini (2007)   | <del>55</del> | <del>14</del> | <del>14</del> |
| Tagua Tagua              | -34.5    | -71.16   | 200   | TERR | Heusser (1990)  | <del>66</del> | <del>14</del> | <del>10</del> |
| Taiquemó                 | -42.17   | -73.6    | 170   | TERR | Heusser et al. (1999); Heusser and Heusser (2006)   | <del>88</del> | <del>00</del> | <del>00</del> |
| Toushe Basin             | 23.82    | 120.88   | 650   | TERR | Liew et al. (2006)  | <del>88</del> | <del>00</del> | <del>00</del> |
| Tswaing Crater           | -25.4    | 28.08    | 1100  | TERR | Partridge et al. (1997); Scott et al. (2008); L. Scott, unpublished data;   | <del>66</del> | <del>04</del> | <del>04</del> |
| Tyrrendara Swamp         | -38.1986 | 141.7626 | 13    | TERR | Builth et al. (2008)  | <del>NA</del> | <del>NA</del> | <del>NA</del> |
| Valle di Castiglione     | 41.9     | 12.76    | 44    | TERR | Alessio et al. (1986); Follieri et al. (1988); Follieri et al. (1989); Narcisi et al. (1992); Narcisi (1999); Magri & Tzedakis (2000); Magri (2008) | <del>77</del> | <del>12</del> | <del>12</del> |
| W8709-13 PC              | 42.11    | -125.75  | -2712 | MARI | Pisias et al. (2001)  | <del>77</del> | <del>12</del> | <del>12</del> |
| W8709-8 PC               | 42.26    | -127.68  | -3111 | MARI | Heusser (1998); Lyle et al. (1992)  | <del>NA</del> | <del>NA</del> | <del>NA</del> |
| Walker Lake              | 35.38    | -111.71  | 2500  | TERR | Berry et al. (1982); Adam et al. (1985); Hevly (1985)   | <del>NA</del> | <del>NA</del> | <del>NA</del> |

616

617

618 Table 2. Leave-out cross-validation (with geographically and climatically close sites removed)  
 619 using fxTWA-PLSv2 for mean temperature of the coldest month (MTCO), mean temperature  
 620 of the warmest month (MTWA) and plant-available water ( $\alpha$ ) with P-splines smoothed  $fx$   
 621 estimation and bins of 0.02, 0.02 and 0.002, respectively.  $n$  is the number of components where  
 622 the last significant number of components is indicated in **bold**. Avg.bias is the average bias;  
 623 RMSEP is the root-mean-square error of prediction; and  $\Delta$ RMSEP is the per cent change of  
 624 RMSEP, which is  $100 \times (\text{RMSEP}_n - \text{RMSEP}_{n-1})/\text{RMSEP}_{n-1}$ ; when  $n = 1$ ,  $\text{RMSEP}_0$  is the  
 625 RMSEP of the null model.  $p$  assesses whether using the current number of components is  
 626 significantly different from using one component less. The degree of overall compression is  
 627 assessed by linear regression of the cross-validated reconstructions on to the climate  
 628 variable;  $b_1$  and  $b_{1.se}$  are the slope and the standard error of the slope, respectively. The closer  
 629 the slope ( $b_1$ ) is to 1, the less the compression.

|           | n        | $R^2$       | Avg.bias     | RMSEP        | $\Delta$ RMSEP | $p$          | $b_1$       | $b_{1.se}$  |
|-----------|----------|-------------|--------------|--------------|----------------|--------------|-------------|-------------|
| MTCO (°C) | 1        | 0.72        | -1.11        | 6.83         | -45.45         | 0.001        | 0.83        | 0.00        |
|           | 2        | 0.74        | -1.21        | 6.68         | -2.25          | 0.001        | 0.84        | 0.00        |
|           | <b>3</b> | <b>0.75</b> | <b>-1.10</b> | <b>6.51</b>  | <b>-2.48</b>   | <b>0.001</b> | <b>0.85</b> | <b>0.00</b> |
|           | 4        | 0.75        | -1.10        | 6.54         | 0.53           | 1.000        | 0.85        | 0.00        |
|           | 5        | 0.75        | -1.13        | 6.54         | -0.07          | 0.188        | 0.85        | 0.00        |
| MTWA (°C) | 1        | 0.54        | -0.33        | 3.89         | -29.76         | 0.001        | 0.66        | 0.00        |
|           | 2        | 0.58        | -0.32        | 3.69         | -5.10          | 0.001        | 0.71        | 0.00        |
|           | <b>3</b> | <b>0.59</b> | <b>-0.33</b> | <b>3.68</b>  | <b>-0.14</b>   | <b>0.001</b> | <b>0.71</b> | <b>0.00</b> |
|           | 4        | 0.59        | -0.33        | 3.69         | 0.07           | 0.746        | 0.71        | 0.00        |
|           | 5        | 0.59        | -0.33        | 3.67         | -0.39          | 0.001        | 0.71        | 0.00        |
| $\alpha$  | 1        | 0.62        | -0.02        | 0.189        | -37.73         | 0.001        | 0.66        | 0.00        |
|           | 2        | 0.63        | -0.022       | 0.188        | -0.81          | 0.001        | 0.68        | 0.00        |
|           | 3        | 0.63        | -0.021       | 0.186        | -0.87          | 0.001        | 0.68        | 0.00        |
|           | <b>4</b> | <b>0.65</b> | <b>-0.02</b> | <b>0.182</b> | <b>-2.11</b>   | <b>0.001</b> | <b>0.71</b> | <b>0.00</b> |
|           | 5        | 0.65        | -0.02        | 0.182        | 0.11           | 1.000        | 0.71        | 0.00        |

630 Table 3: Maximum likelihood estimates of the relationship between the change in mean  
 631 temperature of the coldest month ( $\Delta\text{MTCO}$ ) and the change in mean temperature of the  
 632 warmest month ( $\Delta\text{MTWA}$ ) by latitudinal bands for the northern extratropics (NET, north of  
 633  $23.5^\circ\text{N}$ ), tropics (TROP, between  $23.5^\circ\text{N}$  and  $23.5^\circ\text{S}$ ) and southern extratropics (SET, south of  
 634  $23.5^\circ\text{S}$ ). The intercepts were set to zero since both variables are changes. ~~Coefficients in bold~~  
 635 ~~mean both the lower 95% and upper 95% estimates are above 0.~~

| Region |       | Coefficient                   | Standard error<br>(SE) | Lower 95%               | Upper 95%              |
|--------|-------|-------------------------------|------------------------|-------------------------|------------------------|
| NET    | Slope | <del>2.183</del> <b>2.055</b> | <del>0.334</del> 0.257 | <del>1.528</del> 1.551  | <del>2.838</del> 2.560 |
| TROP   | Slope | <del>1.427</del> 0.983        | <del>0.509</del> 0.551 | <del>0.430</del> -0.098 | <del>2.425</del> 2.064 |
| SET    | Slope | <del>1.665</del> <b>1.849</b> | <del>0.575</del> 0.772 | <del>0.538</del> 0.336  | <del>2.791</del> 3.363 |

636

637

638 Table 4: Maximum likelihood estimates of the relationship between the change in plant-  
 639 available water ( $\Delta\alpha$ ) and the change in mean temperature of the warmest month ( $\Delta\text{MTWA}$ ) by  
 640 latitudinal bands for the northern extratropics (NET, north of 23.5°N), tropics (TROP, between  
 641 23.5°N and 23.5°S) and southern extratropics (SET, south of 23.5°S). The intercepts were set  
 642 to zero since both variables are changes. ~~Coefficients in bold mean both the lower 95% and~~  
 643 ~~upper 95% estimates are above 0.~~

| Region |       | Coefficient                   | Standard error<br>(SE)        | Lower 95%                     | Upper 95%                     |
|--------|-------|-------------------------------|-------------------------------|-------------------------------|-------------------------------|
| NET    | Slope | <del>0.069</del> <b>0.066</b> | <del>0.011</del> <b>0.009</b> | <del>0.048</del> <b>0.048</b> | <del>0.091</del> <b>0.084</b> |
| TROP   | Slope | <del>0.077</del> <b>0.059</b> | <del>0.010</del> <b>0.020</b> | <del>0.058</del> <b>0.019</b> | <del>0.095</del> <b>0.098</b> |
| SET    | Slope | <del>0.054</del> <b>0.071</b> | <del>0.014</del> <b>0.020</b> | <del>0.027</del> <b>0.032</b> | <del>0.082</del> <b>0.110</b> |

644